ARL-TR-8452 ● AUG 2018

US Army Research Laboratory

Assessing X-ray Contamination from Neighboring Sources in the US Army Research Laboratory's (ARL's) Multi-Energy Flash Computed Tomography Diagnostic

by MB Zellner, J Perrella, D Schall, A Ducote, T Nellenbach, T O'Connor, T Quigg, and N Sturgill

Approved for public release; distribution is unlimited.

NOTICES

Disclaimers

The findings in this report are not to be construed as an official Department of the Army position unless so designated by other authorized documents.

Citation of manufacturer's or trade names does not constitute an official endorsement or approval of the use thereof.

Destroy this report when it is no longer needed. Do not return it to the originator.

ARL-TR-8452 ● AUG 2018

US Army Research Laboratory

Assessing X-ray Contamination from Neighboring Sources in the US Army Research Laboratory's (ARL's) Multi-Energy Flash Computed Tomography Diagnostic

by MB Zellner, D Schall, and A Ducote
Weapons and Materials Research Directorate, ARL

J Perrella, T Nellenbach, T O'Connor, T Quigg, and N Sturgill
Bowhead Total Enterprise Solutions, Alexandria, VA

Approved for public release; distribution is unlimited.

REPORT DOCUMENTATION PAGE

Form Approved
OMB No. 0704-0188

Public reporting burden for this collection of information is estimated to average 1 hour per response, including the time for reviewing instructions, searching existing data sources, gathering and maintaining the data needed, and completing and reviewing the collection information. Send comments regarding this burden estimate or any other aspect of this collection of information, including suggestions for reducing the burden, to Department of Defense, Washington Headquarters Services, Directorate for Information Operations and Reports (0704-0188), 1215 Jefferson Davis Highway, Suite 1204, Arlington, VA 22202-4302. Respondents should be aware that notwithstanding any other provision of law, no person shall be subject to any penalty for failing to comply with a collection of information if it does not display a currently valid OMB control number.
PLEASE DO NOT RETURN YOUR FORM TO THE ABOVE ADDRESS.

1. REPORT DATE *(DD-MM-YYYY)*	**2. REPORT TYPE**	**3. DATES COVERED (From - To)**
August 2018	Technical Report	1 October 2017–31 July 2018

4. TITLE AND SUBTITLE

Assessing X-ray Contamination from Neighboring Sources in the US Army Research Laboratory's (ARL's) Multi-Energy Flash Computed Tomography Diagnostic

5a. CONTRACT NUMBER

5b. GRANT NUMBER

5c. PROGRAM ELEMENT NUMBER

6. AUTHOR(S)

MB Zellner, J Perrella, D Schall, A Ducote, T Nellenbach, T O'Connor, T Quigg, and N Sturgill

5d. PROJECT NUMBER

AH80

5e. TASK NUMBER

5f. WORK UNIT NUMBER

7. PERFORMING ORGANIZATION NAME(S) AND ADDRESS(ES)

US Army Research Laboratory
Weapons and Materials Research Directorate (ATTN: RDRL-WMP-E)
Aberdeen Proving Ground, MD 21005

8. PERFORMING ORGANIZATION REPORT NUMBER

ARL-TR-8452

9. SPONSORING/MONITORING AGENCY NAME(S) AND ADDRESS(ES)

10. SPONSOR/MONITOR'S ACRONYM(S)

11. SPONSOR/MONITOR'S REPORT NUMBER(S)

12. DISTRIBUTION/AVAILABILITY STATEMENT

Approved for public release; distribution is unlimited.

13. SUPPLEMENTARY NOTES

14. ABSTRACT

The US Army Research Laboratory and Lawrence Livermore National Laboratory have recently constructed a Multi-Energy Flash Computed Tomography (MEFCT) diagnostic. The device uses multiple flash X-ray systems to acquire projection data of dynamic events from multiple perspectives. These views are then combined to compute three independent, time-sequenced volume reconstructions of the event. Since multiple source/detector pairs are used to collect the projection data, X-ray photons from some sources often contaminate neighboring detectors. This contamination is unique to the MEFCT system in the way it collects projection data and acts to complicate the mathematical reconstruction process and reduce the diagnostic's overall resolution. This work assesses the neighbor source contamination and mathematically generates a set of correction images from an empirical dataset where multiple independent contamination events occurred. The correction images are then to be subtracted from the attenuation radiographs prior to the tomographic reconstruction to improve reconstruction quality.

15. SUBJECT TERMS

X-radiography, computed tomography, flash radiography, Beer–Lambert

16. SECURITY CLASSIFICATION OF:			**17. LIMITATION OF ABSTRACT**	**18. NUMBER OF PAGES**	**19a. NAME OF RESPONSIBLE PERSON**
a. REPORT	**b. ABSTRACT**	**c. THIS PAGE**			Michael B Zellner
Unclassified	Unclassified	Unclassified	UU	20	**19b. TELEPHONE NUMBER (Include area code)** (410) 306-2565

Standard Form 298 (Rev. 8/98)
Prescribed by ANSI Std. Z39.18

Contents

List of Figures

List of Tables

1. Introduction

X-ray computed tomography is a powerful technique for visually, and physically, understanding a dynamic system throughout three spatial dimensions.[1,2] With the advent of the US Army Research Laboratory's (ARL's) Multi-Energy Flash Computed Tomography (MEFCT) system,[3–5] X-ray tomography has increased its capability to track mass flux through a reconstruction volume, without the constraint that the mass be elastically bound.[6] This capability has the potential to improve our understanding of dynamic systems such as fuel injection flow inside an internal combustion engine or fragmentation of targets during ballistic impacts. To extend this technique's capability in the temporal dimension, hardware modifications were incorporated to compensate for conventional capabilities' deficiencies. One hardware modification included is the use of multiple broadband X-ray flash systems to simultaneously collect multiple views of the event. This is done by physically mounting 15 X-ray sources and 15 X-ray detectors on three interlaced spheres of approximately 2 m in diameter, to assess a target held at the sphere's center. This modification solved the temporal aspect of collecting the many views for the reconstruction process in a timely manner but caused additional complications that degrade the quality of the volume reconstruction when not sufficiently accounted for.

Generally, in X-ray computed tomography, a reconstructed volume space is computed by mathematically inferring what orientation some scattering medium must have occupied during multiple 2-D X-ray scattering events of varying perspectives. Typically the process of collecting the scattering projections occurs serial in time, collecting projection 1, followed by projection 2, and so on until sufficient projections are collected. For each subsequent projection, either the target is rotated to give a slightly different angular perspective, or the target remains still and the X-ray source/detector pair is rotated about the center of the target axis to achieve a similar effect. The multiple perspectives are then combined using a computer-aided routine to represent the data in a 3-D volume. Multiple routines are available, each with benefits and weaknesses. The original routines were based on the theory of applying a Radon Transform[7] to analytically correlate projection data to the scattering body. Solving the system of linear equations necessary to compute a volume reconstruction using this method was relatively efficient in computational time but required many views (>1000 in some cases) for sufficient 3-D resolution.[7–9] Newer routines use advanced iterative methods that compare the attenuation from some hypothetical scattering volume to that detected by each projection from their unique perspective. These routines then modify the hypothetical scattering volume based on a correction method and iterate until some

minimization criterion is reached. These methods are usually more computationally expensive but reduce the number of perspectives needed.[10–13]

The MEFCT device takes advantage of iterative routines that require fewer views, using only five views per reconstruction. The multi-perspective data are analyzed using a combination of custom preprocessing scripts written in MATLAB and reconstructed using a specialized iterative routine within Livermore Tomography Tools (LTT).[13] Since the system uses only five views, it is very sensitive to the attenuation levels detected in each perspective. This is complicated by the fact that the system uses multiple source/detector systems to collect all five views at the same time (within a 100-ns window), and X-ray photons from some sources often contaminate neighboring detectors. Here, we perform a thorough analysis of where the neighboring X-rays originate, where they are detected, and how to compensate for them mathematically when sufficient shielding is not practical.

2. Results

Within LTT, the iterative routine compares the attenuation computed from a hypothetical scattering object to that detected by the measured projection views. The attenuation is derived from the Beer–Lambert law and defined as

$$g = -\log\left(c * max\left(\frac{(I - I_{dark})}{(I_{background} - I_{dark})}\right)\right), \quad (1)$$

where g is the attenuation data, c is a constant obtained by sampling the image using a "postage-stamp" routine*, I is the dynamic radiograph image, $I_{\text{background}}$ is the background radiograph image, and I_{dark} is the dark field image.

In typical X-ray computed tomography systems, I, $I_{\text{background}}$, and I_{dark} are easily acquired. In fact, since typical devices only contain one source and one detector, single $I_{\text{background}}$ and I_{dark} images can be used to compute the attenuation for each dynamic frame. In the MEFCT diagnostic, however, contamination of X-rays from a source onto nearby detectors occurs because multiple criteria are all met:

- The X-ray detectors are Carestream Health GP Digital Imaging Plates, which can acquire X-ray photon counts at any time (as an analogy, they behave as a photographic camera that has an open shutter at all times).
- The X-ray sources are flash sources that have a large solid angle distribution of X-ray photon emission.

* This multiplicative constant is used to baseline the data using a reference area where no scattering object is known to be in the field of view. In an ideal case, $c = 1$. If not ideal, c is set to the reciprocal of the mean of the transmission data over the selected region.

- Many X-ray sources are used in near proximity to other sources and detectors.
- Complete shielding of the detectors from neighboring source X-ray photons is not practical because of the relatively high peak X-ray photon energy (150 to 450 keV).

Figure 1A shows the X-radiation dose measured using a pencil dosimeter located 1 m from the arc discharge location of the X-ray system diode. The measurements were performed throughout 180°, with 0° being registered to directly in front of the tube source. Figure 1B extrapolates this dose to a field view assuming cylindrical symmetry around the source. Figure 2 shows a computer-aided drawing of the MEFCT support structure indicating the location of multiple X-ray sources and detectors. As an eye-guide, two neighboring X-ray systems are highlighted in red and green, respectively. The sources are depicted as cylinders, and the detectors are depicted as rectangular prisms. From these images, it can be envisioned how the X-ray dose from one source (green) will contaminate the neighboring detector (red) if not sufficiently shielded. Because this dose is not from the desired source, it alters the apparent attenuation that would have been incurred by an object located at the center of the MEFECT structure. This contamination hinders the reconstruction process and therefore must be accounted for. Because the contamination relates photons that are not involved in the scattering process, this effect can be compensated for by adjusting the I_{dark} images of Eq. 1 using the substitution

$$I^{n}_{dark} = I^{n}_{dark\ detector} + \sum_{i=1}^{15} I^{i,i\neq n}_{contamination}\ , \qquad (2)$$

where $I^{\text{n}}_{\text{dark detector}}$ is the conventional dark field image of the n$^{\text{th}}$ X-ray system when no external contamination is present, which relates efficiencies of the X-ray imaging plate and scanner process, and $I^{\text{i}}_{\text{contamination}}$ relates the contamination effects on the n$^{\text{th}}$ system's detector from the i$^{\text{th}}$'s X-ray source.

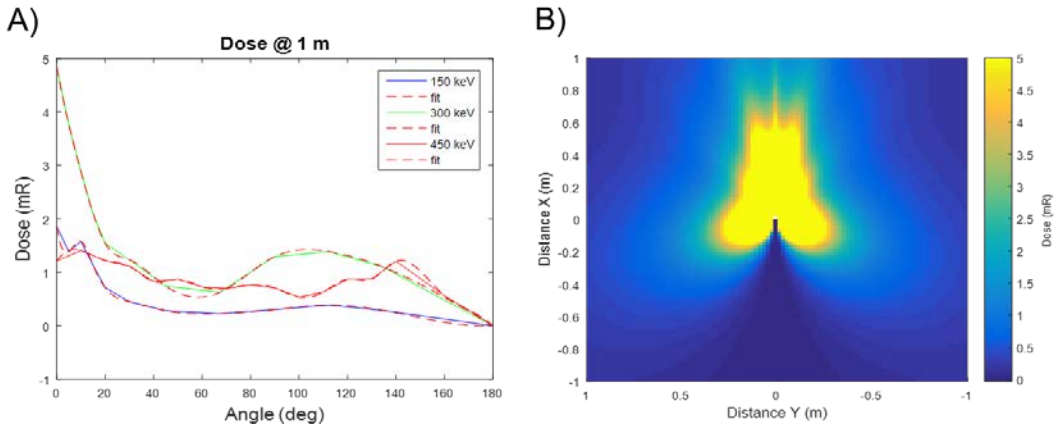

Fig. 1 A) Radiation dose measured from the 150-, 300-, and 450-keV sources as a function of angle off of the principal axis and B) an x-y slice of the radiation field acquired by extrapolating the 150-keV dose measurement fit using cylindrical symmetry

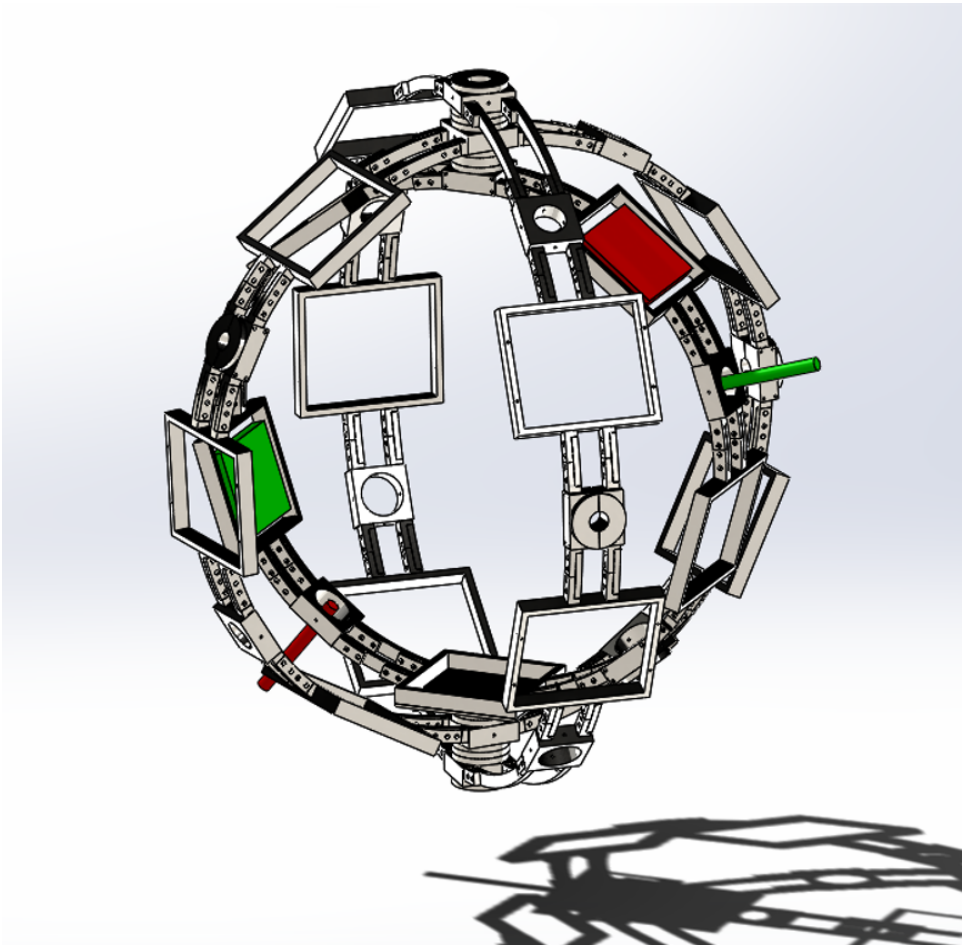

Fig. 2 Computer-aided drawing of the MEFCT system support structure. In this rendering, the inner system 2 is highlighted by green tones and the inner system 4 is highlighted by red tones. The X-ray sources are cylindrical tubes, and the X-ray detectors are flat, rectangular panels.

Approved for public release; distribution is unlimited.

To demonstrate the magnitude of the contamination, Fig. 3 shows multiple views of the inner system 4 detector imaging plate (red rectangular prism in Fig. 2) when exposed to different circumstances of source illuminations and processing methodologies. These images have been independently contrast adjusted to help visualize gradients (max value white, minimum value black). The top-row center-column image labeled "Dark, 4.4374" depicts the imaging plate when scanned without any exposure to X-rays. This is the conventional $I_{\text{dark detector}}$. The number 4.4374 represents the mean pixel value of the 16-bit image (minimum 0, maximum 65535). The top-row left-column image is the signal recorded on the detector of the inner system 4 detector when only inner source 2 (green cylinder in Fig. 2) was illuminated. Here the mean value jumps to 4.9939, and one can clearly see additional counts (whiter pixels) along the image's right edge. For reference, the bottom-row, right-column image was collected when only inner source 4 (red cylinder in Fig. 2) was illuminated. It has a mean pixel value of 54.6977. A simple correlation suggests that the contamination from a single source is near 1%, and when summed over, all 14 nonactive heads could contribute to a significant influence on the attenuation calculation.

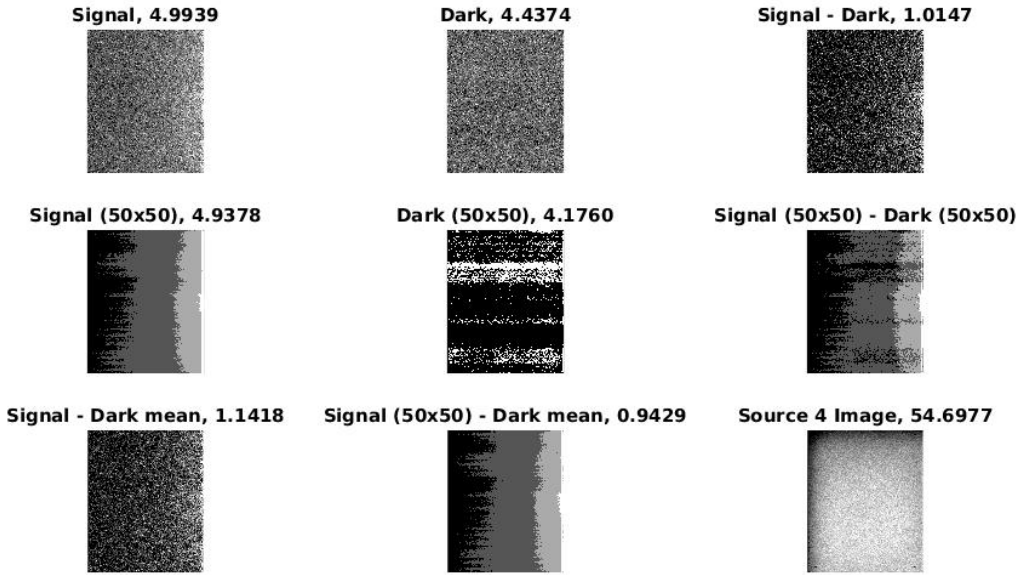

Fig. 3 Images of the inner system 4 detector (red rectangular prism in Fig. 2) imaging plate for multiple circumstances of source illuminations and processing methodologies. These images have been independently contrast adjusted to help visualize gradients (max value white, minimum value black). Image plate scans labeled "Dark" have not been illuminated by any source; they represent dark current values of the scanner and scanning process (labeled "Dark Detector" in the text and equations). Image plate scans labeled "Signal" were acquired after the neighboring source inner system 2 (green cylinder in Fig. 2) was illuminated, with no other systems illuminating. The image labeled "Source 4 Image" is that where only the inner system 4 (red cylinder in Fig. 2) source was illuminated and represents average signal strength and beam shape when no target is included. The number following each image title represents the noncontrast-adjusted image mean pixel values (16-bit gray scale).

Empirically, one could collect the desired I^{n}_{dark} images directly by simultaneously flashing all sources except for the n^{th} and read out the corresponding detector.[*] This measurement could then be repeated for each source. However, this would add an undesirable stress onto the system in that each source would incur 14 flashes to collect the entire data set.[†] This report describes two alternative methods to account for all contamination possibilities that impose less system stress than the direct measurement. In the first method, an empirical data set is collected in which each source is illuminated independently, resulting in only one flash per system total. In this method, the I^{n}_{dark} images are computed using the summation-based method described by Eq. 2 after separating out detector and contamination contributions. In the second method, an additional full-system flash is acquired simultaneously. These data are combined with the data of the first set using a subtraction-based method to produce the I^{n}_{dark} images. This method results in a total of two flashes per system.

3. Method 1: Summation of Independent Contributions

For this method, a data set was collected in which each source was illuminated independently. After each illumination, all detectors were measured. Each measured output from this method, however, does not relate any of the singular quantities desired in Eq. 2. Instead, each measured output relates the quantity:

$$I_{signal} = I^{n}_{dark\ detector} + I^{i}_{contamination}\,. \tag{3}$$

To separate variables and attain the $I^{i}_{\text{contamination}}$ terms independently so that we can compute the sum desired by Eq. 2, we must subtract the $I^{n}_{dark\ detector}$ contribution from each I_{signal} measurement:

$$I^{i}_{contamination} = I_{signal} - I^{n}_{dark\ detector}\,. \tag{4}$$

If we do this directly, because of the image pixilation, we approximately double the image noise. This is depicted in the top-row right-column of Fig. 3. We can reduce the image noise by filtering the images with a median-square filter prior to performing mathematical operations. Examples of this performed with a 50 × 50 median filter are shown in Fig. 3 for the signal image and the dark (detector) image (middle-row left-column and middle-row center-column, respectively). A simple subtraction of these gives a significantly enhanced signal-to-noise ratio of the contamination signal as shown in the middle-row right-column panel.

[*] All methods described in this report assume that the system dose is consistent between flashes. In reality, the dose has slight shot-to-shot variability, which can cause issues when using difference methods to attain attenuation images. Examples are detailed later in this report.

[†] Thermal aspects of each flash slightly erode the tungsten anode of the X-ray diode.

We can enhance the signal-to-noise ratio further if instead of the median-filtered dark detector image, we subtract the median dark detector pixel value:

$$I^{i}_{contamination} \cong I_{signal} - I^{n}_{dark\ detectro\ mean\ value}. \quad (5)$$

This is shown in the bottom-row center-column panel. This process produces a mean pixel value very similar to the value generated by subtracting the original dark detector from the signal images. Here we note that if the corruption signal were to be rather low, the filtered corruption signal less the dark detector pixel value would produce an image that has a significant structure on the order of 1 or 2 bits dynamic range. If many of these were summed together as necessitated by Eq. 2, the resulting image could have substantial noise. This phenomenon is detectable in Fig. 4, which shows a compilation of all the I_{dark} images for each X-ray system generated using the summation of independent contributions method. Although significant low-frequency features (those of the contamination) are detected, substantial noise is seen (typically as horizontal and vertical bands) throughout.

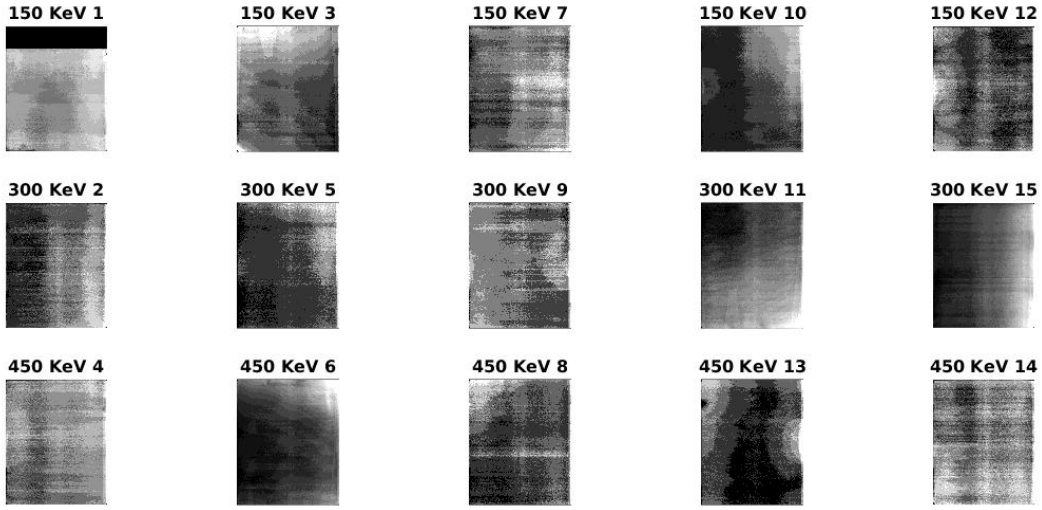

Fig. 4 Synthetic I_{dark} images demonstrating contamination effects. These images were computed by summing the contamination effects measured on detectors exposed to individual X-ray sources.

4. Method 2: Source Subtraction

A second method to obtain the contamination profile for the nth system would be to acquire an image in which all sources were illuminated at a single instance, and then to subtract the contributions of the nth source (an example of which is shown in the bottom-row right-column of Fig. 3). When collecting the images with all sources illuminated simultaneously, one obtains images where

$$I_{signal\ simultaneous} = I^{n}_{dark\ detector} + \sum_{i=1}^{15} I^{i,i\neq n}_{contamination} + I^{n}_{source}. \quad (6)$$

Note the I^n_{source} nomenclature is used instead of $I^{i=n}_{contamination}$ to emphasize that this contribution comes from the desired source. To compute to the I^n_{dark} images, one simply needs to subtract the I^n_{source} term, which is measured during the individual flashes:

$$I^n_{dark} = I^n_{signal\ simultaneous} - I^n_{source}. \tag{7}$$

To obtain this data, a single extra flash would be added to each system (physically all performed at the same time). Figure 5 shows the compilation of this method's computed I_{dark} images for each X-ray system.

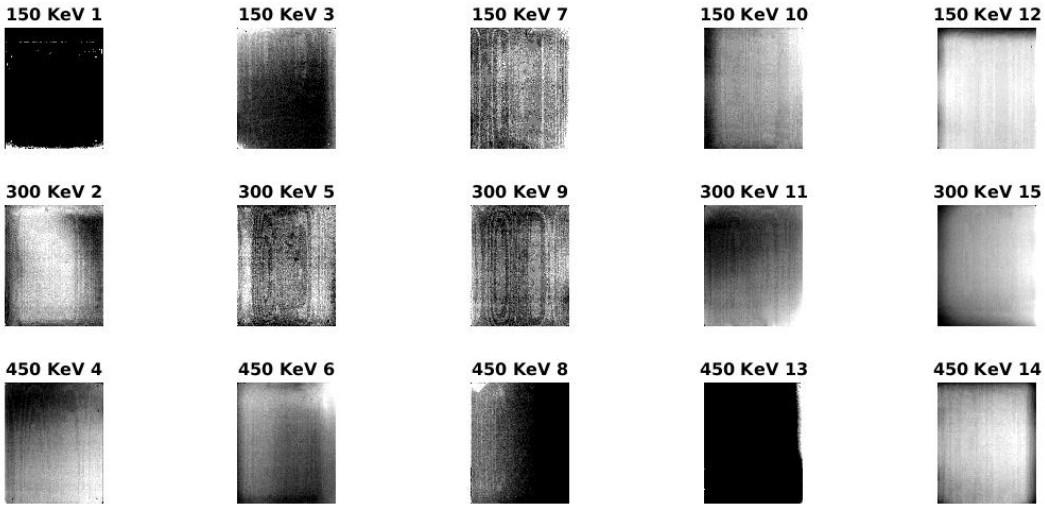

Fig. 5 Synthetic I_{dark} images demonstrating contamination effects. These images were computed by subtracting the signal measured by detectors when individual X-ray source exposures were conducted from measurements where all X-ray sources were illuminated simultaneously.

5. Discussion

Table 1 shows a comparison of I_{dark} images when computed using the two methods. Generally, the contamination patterns match between both methods. For example, the 150-keV 3 system displays contamination in the upper-right corner of the image plate with both methods. However, both analysis methods have strengths and weaknesses in making the assessment. Although the summation of independent contributions method incurs a significant amount of noise, it is rooted using a difference term where the remaining signal is near or greater than the magnitude of the signal subtracted. In the source subtraction method, the difference term involves removing a significant portion of the total measured signal, making it much more susceptible to X-ray intensity fluctuations. This is most notable in images labeled 150-keV 1 and 450-keV 13, where the X-ray intensity must have been greater in the individual flashes than in the simultaneous flash, resulting in an array of zeros

(negative numbers are truncated) and elimination of the signal. Because of this effect, the first method is suggested for use during analysis.

Table 1 Comparison of I_{dark} images when computed using both methods

I_{dark}	Method 1				Method 2			
	Mean	**Min**	**Max**	**RMS**	**Mean**	**Min**	**Max**	**RMS**
1	9.95	0	17	10.41	0.05	0	63	0.43
2	13.36	0	22	13.45	11.55	0	37	11.82
3	14.51	0	23	14.63	2.42	0	54	3.37
4	14.75	0	23	14.81	12.84	0	48	13.61
5	9.51	0	17	9.59	10.44	0	40	10.56
6	16.99	0	38	17.29	13.17	0	65	13.85
7	12.89	0	21	12.96	5.07	0	32	5.15
8	11.59	0	18	11.64	1.89	0	74	4.50
9	11.83	0	19	11.87	9.19	0	39	9.38
10	9.35	0	19	9.51	15.41	0	24	15.65
11	18.44	0	38	18.82	10.02	0	58	10.72
12	11.97	0	19	12.04	35.17	0	47	35.49
13	7.16	0	15	7.25	0.20	0	102	1.47
14	23.13	0	29	23.19	39.31	0	47	39.57
15	19.53	0	40	20.08	34.03	0	56	34.97

Note: RMS = root mean squared.

To demonstrate the effectiveness of correcting for neighbor contamination through modification of the I_{dark} term, two reconstructions were computed for an experiment where a bullet impacted an aluminum plate. In the first reconstruction, the I_{dark} data that contained only information that relates efficiencies of the X-ray imaging plate and scanner process were used (i.e., $I_{dark} = I_{dark\ detector}$). In the second reconstruction, compensation for the neighboring contamination was accounted for using Eq. 1 with the summation of independent contributions method (the I_{dark} images shown in Fig. 4). Resulting reconstruction volumes are shown in Fig. 6, with the neighbor contamination being accounted for in the right panel image of the figure. In both images, the same 1-D transfer functions and opacity maps were used. It is evident from these images that the neighbor contamination significantly alters the reconstruction process, resulting in projection of mass to the exterior of the reconstruction volume, represented here by a loss of mass as its quantity falls below the thresholds set by the 1-D transfer function and opacity maps.

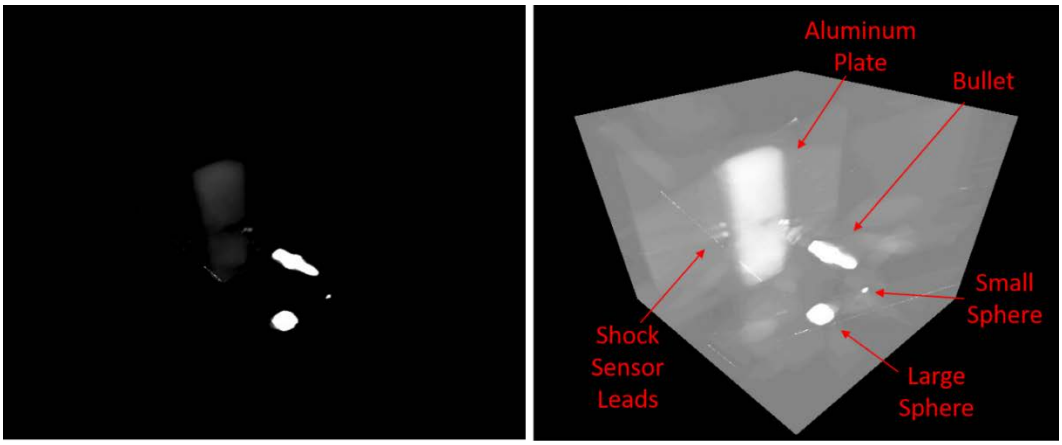

Fig. 6 Resulting reconstruction volumes are those constructed without (left panel) and with (right panel) the neighbor contamination being accounted for using the first method of compensation (Fig. 4). In both images, the same 1-D transfer functions and opacity maps were used. For scale, the large sphere composed of steel is 12.7 mm in diameter, and the small sphere composed of lead is 2 mm in diameter.

6. Conclusions

To accurately perform X-ray computed tomography using the MEFCT diagnostic, accommodations must be made to correct for neighboring source X-ray contamination. This contamination is a direct result of the need to use multiple flash X-ray systems and detectors, simultaneously, in near proximity to each other. In order to correct for the contamination, we have made accurate measurements of this contamination, while imposing minimal stress on the individual X-ray systems. Measurements demonstrated that individual neighbor contributions could be as high as 1%–2% of the total signal, and the total neighbor contamination could be near 20% of the total signal (see Table 1). To compute synthetic dark images for each system, which can be applied to solve for the dark image variable within the Beer–Lambert law, we proposed two methods to separate easily made but compounded measurements into singular variables. Although the first method incurs a significant amount of noise, it is rooted using a difference term where the remaining signal is near or greater than the magnitude of the signal subtracted. In the second method, a difference term involves removing a significant portion of the total measured signal, making it much more susceptible to X-ray intensity fluctuations. Because the second method is sensitive to X-ray flux, the first method is suggested to be employed. Use of either method, however, will allow for a more accurate computation of the attenuation image.

7. References

1. Herman GT. Fundamentals of computerized tomography: image reconstruction from projections. 2nd ed. Dordrecht (Netherlands): Springer; 2009. ISBN 978-1-85233-617-2.

2. Moser S, Nau S, Manfred S, Klaus T. In situ flash X-ray high-speed computed tomography for the quantitative analysis of highly dynamic processes. Meas. Sci Technol. 2014;25:025009.

3. Zellner MB, Chaney GT, Benjamin CA, Cantrell R, Borys RW, Strickland RD, Sturgill JM, Perrella JA, Schafer GL, Yonce CE, et al. Considerations for the design of a multi-color high-speed x-ray computed tomography diagnostic. Army Research Laboratory (US); 2014 June. Report No.: ARL-TR-6969.

4. Zellner MB, Randow CL, Cantrell R, Yonce CE. Blast-loading assessment of Multi-Energy Flash Computed Tomography (MEFCT) diagnostic. Army Research Laboratory (US); 2016 Aug. Report No.: ARL-TR-7741.

5. Zellner MB, Champley K, McMichael L, Martz H, Cantrell R, Yonce CE, Dudeck KW, Benjamin CA, Borys RW, Schall DR, et al. Development of a Multi-Energy Flash Computed Tomography diagnostic for three dimensional imaging of ballistic experiments. Proceedings of the Shock Compression of Condensed Matter Topical Group Meeting of the American Physical Society; 2017 July 9–14; St Louis, MO.

6. Zellner MB and Champley K. Development of a computed tomography system capable of tracking material flux through a reconstruction volume. Rev Sci Instr. Forthcoming 2018 submission.

7. Radon J. Uber die bestimmung von funktionen durch ihre integralwerte langs gewisser mannigfaltigkeiten [On the determination of functions from their integrals along certain manifolds]. IEEE Trans Med Imag. 1986 Dec 1;5(4):170–176. Reprint: Ber Saechsische Akad Wiss. 1917;191729:262. doi:10.1109/TMI.1986.4307775. PMID 18244009.

8. Kaczmarz S. Angenäherte auflösung von systemen linearer gleichungen. bulletin international de l'académie polonaise des sciences et des lettres. classe des sciences mathématiques et naturelles. Série A. Sciences Mathématiques. 1937;35:355–357.

9. Gordon R, Bender R, Herman G. Algebraic reconstruction techniques (ART) for three dimensional electron microscopy and X-ray photography. J Theor Bio. 1970;29(3):471–481. doi:10.1016/0022-5193(70)90109-8, PMID 5492997.

10. Mishra D, Longtin JP, Singh RP, Prasad V. Performance evaluation of iterative tomography algorithms for incomplete projection data. Appl Optics. 2004;43(7):1522.

11. Mishra D, Muralidhar K, Munshi P. A robust MART algorithm for tomographic applications. Num Heat Transfer, Part B Fundamentals. Int J Comp Meth. 1999;35(4):485–506.

12. Sidky EY, Pan X. Image reconstruction in circular cone-beam computed tomography by constrained, total-variation minimization. Phys Med Biol. 2008;53:4777–4807.

13. Champley K. Livermore tomography tools (LTT). Livermore (CA): Lawrence Livermore National Laboratory; 2016 Mar. Technical Manual No.: LLNL-SM-687016.

List of Symbols, Abbreviations, and Acronyms

1-/2-/3-D	one-/two-/three-dimensional
ARL	US Army Research Laboratory
MEFCT	Multi-Energy Flash Computed Tomography
LTT	Livermore Tomography Tools
RMS	root mean squared

1 (PDF) DEFENSE TECHNICAL INFORMATION CTR DTIC OCA

2 (PDF) DIR ARL
IMAL HRA
RECORDS MGMT
RDRL DCL
TECH LIB

1 (PDF) GOVT PRINTG OFC
A MALHOTRA

8 (PDF) ARL
RDRL WMP D
M B ZELLNER
J PERRELLA
RDRL WMP E
D SCHALL
A DUCOTE
T NELLENBACH
T O'CONNOR
T QUIGG
N STURGILL